Interaction and dynamics of ionic liquids based on Choline and amino-acids anions.

M. Campetella,[†] E. Bodo,[*,†] R. Caminiti,[*,†] A. Martino,[†] F. D'Apuzzo,[‡] S. Lupi,[¶,§] and L. Gontrani[†]

Dept. of Chemistry, University of Rome "La Sapienza", Italy, CNR-IOM and Dept. of Physics, University of Rome "La Sapienza", Italy, and Dept. of Physics, University of Rome "La Sapienza", Italy

E-mail: enrico.bodo@uniroma1.it; ruggero.caminiti@uniroma1.it

[*]To whom correspondence should be addressed
[†]Dept. of Chemistry, University of Rome "La Sapienza", Italy
[‡]CNR-IOM and Dept. of Physics, University of Rome "La Sapienza", Italy
[¶]Dept. of Physics, University of Rome "La Sapienza", Italy
[§]also: Center for Life Nano Science@Sapienza, Italian Institute of Technology, Rome, Italy

Abstract

The combination of amino acids anions with the choline cation gives origin to a new and potentially important class of organic ionic liquids that might represent a viable and bio-compatible alternative with respect to the traditional ones. We present here a detailed study of the bulk phase of the prototype system composed by the simplest aminoacid (alanine) anion and the choline cation, based on *ab initio* and classical molecular dynamics. Theoretical findings have been validated by comparing with accurate experimental X-ray diffraction data and infrared spectra. We find that hydrogen bonding (HB) features in these systems are crucial in establishing their local geometric structure. We have also found that these HBs once formed are persistent and that the proton resides exclusively on the choline cation. In addition, we show that a classical force field description for this particular ionic liquid can be accurately performed by using a slightly modified version of the *Gaff* force field.

Introduction

Ionic liquids (ILs) are a class of useful and interesting materials for a variety of both scientific and applicative issues.[1–3] Their low vapor pressure and their high thermal and chemical stabilities[4] makes them a potential replacement for typically polluting volatile organic solvents. In addition the high number of available cation-anion combinations allows, by changes in the nature of the constituents ionic species, to provide materials with highly tunable chemical and physical properties. Their peculiar chemical and physical properties stem from the complexity and from the strength of the nanoscopic interactions between their molecular constituents that include long-range isotropic Coulombic forces and short-range van der Waals ones. In ad- dition, many ionic liquids, such as the ones considered here, are also characterized by the presence of strong and anisotropic hydrogen bonds[5–8] which provide an environment that is reminiscent of the complex interaction networks that we are used to find in protic solvents such as water.

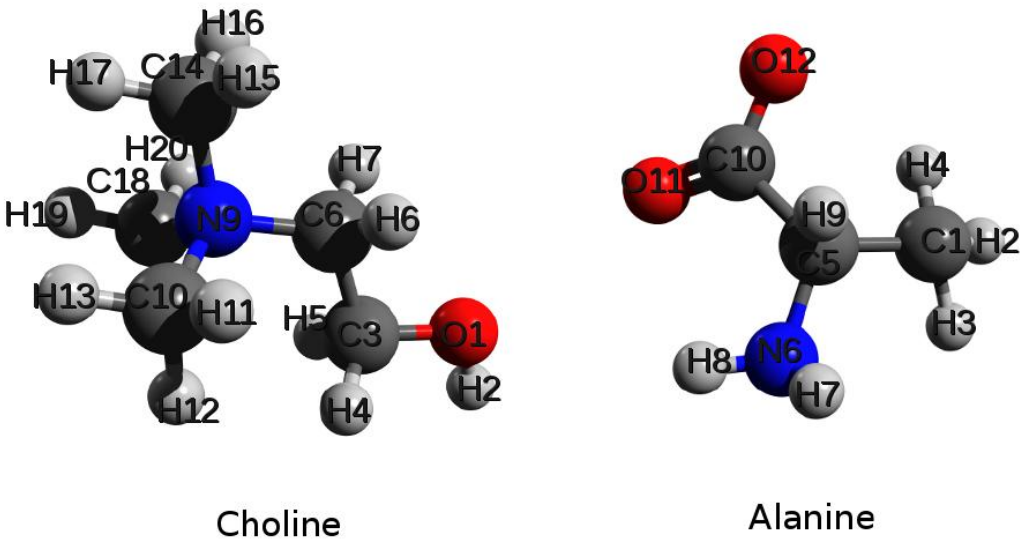

Figure 1: Representation of Choline cation and Alanine anion with their reference atom labels.

The new class of compounds explored here through the analysis of one of its representatives, has been usually considered non-noxious and therefore suitable for green chemistry processes from the early days of their appearance. They have been subjected to toxicity studies at several biological levels in order to evaluate the risks to the environment from their use in production processes.[9–15] These materials are generally composed of cations and anions derived from biomaterials such as amino acids, ammonium, guanidinium and cholinium ions. In particular, it has already been shown that the class of ILs produced from choline were found to have low toxicity to humans and to the environment,,[10,14,16] so that they are considered to be a promising class of materials for a wide range of uses. More specifically the combination of choline with amino-acids anions has been recently exploited to provide non toxic ionic liquids.[17–21]

In order to characterize one of the prototype in this series of compounds, we present here a study in which we employ a combination of *ab initio* molecular dynamics (MD), classical MD and experimental measurements with the aim of interpreting the geometric structure and the dynamics of the corresponding bulk liquid systems. In particular we have chosen as the subject of this study the ion pair composed by the choline cation $[Cho]^+$ and alanine anion $[Ala]^-$. As we shall see in the following, we have initially focused our interest on the structural characterization of the liquid with particular attention to the HB interaction occurring between the ion couples. In order to provide a validation of the theoretical data we have compared the findings from the MD simulations to the measured X-ray diffraction patterns and infrared spectra of the bulk liquid. These data, as far as we know, have been presented here for the first time.

Experimental details

X-Ray Diffraction

The large angle X-ray scattering experiments were performed at room temperature using the noncommercial energy-scanning diffractometer built in the Department of Chemistry at the University 'La Sapienza' of Rome (Italian Patent No. 01126484-23 June, 1993). For a detailed description of instrument, technique, and the experimental protocol of the data acquisition phase, the reader is referred to Refs.[22–25] In this experiment, the new $0-2\theta$ instrument geometry (only one of the two diffractometer arms can move) was used; the samples were prepared and put in 2-mm quartz cylindrical capillaries, immediately after a 72-h drying in high vacuum pump. In such setup, higher diffracted intensities can be recorded. The diffraction patterns acquired at the different angles were then joined to obtain a continuous spectrum in Q; only five diffraction angles are enough to cover a Q-spectrum ranging from 0.1 to 19.56 Å^{-1}. The total intensity of the radiation scattered by the sample, after the correction for systematic effects (polarization, absorption, and incoherent scattering) and rescaling to absolute units (electron units per stoichiometric unit), can be expressed as the sum of two terms:

$$I_{EXP}(Q)_{E.U.} = \sum_{i=1}^{N} x_i f_i^2 + I(Q). \quad (1)$$

The first term represents the independent atomic scattering from the atoms in a stoichiometric unit, while I(Q) is the 'total (static) structure factor' and constitutes the structurally sensitive part of the scattering intensity, being due to the interference contributions from different atoms. The variable Q is the magnitude of the transferred momentum, and depends on the scattering angle (2θ), according to the relation Q = 4π (sin $\frac{\lambda}{\theta}$), which is equal to Q $\approx$ 1.0136 E sin θ, if E is expressed in keV and Q in Å^{-1}. The function I(Q) is related to the

pair correlation functions descriptive of the structure, according to the formula:

$$I(Q) = \sum_{i=1}^{N} \sum_{j=1}^{N} x_i x_j f_i f_j H_{ij}(Q), \tag{2}$$

where we have introduced the partial structure functions H_{ij} defined in terms of the atom-atom radial distribution functions (RDFs) by the following Fourier integral:

$$H_{ij}(Q) = 4\pi\rho_0 \int_0^{\infty} r^2 (g_{ij}(r) - 1) \frac{sinQr}{Qr} dr, \tag{3}$$

where ρ_0 is the bulk number density of the system, x_i are the numerical concentrations of the species and f_i their Q-dependent X-ray scattering factors.

Both the experimental and theoretical structure functions have been multiplied by a modification function

$$M(Q) = \frac{f_N^2(0)}{f_N^2(Q)} exp^{-0.01Q^2} \tag{4}$$

that is necessary to improve the curve resolution at high Q, and then Fourier-transformed into a radial distribution function ($D(r)$), according to the relation

$$D(r) - 4\pi\rho^2 = \frac{2r}{\pi} \int_0^{\infty} QI(Q)M(Q)sin(Qr)dQ. \tag{5}$$

If the $4\pi\rho^2$ term of the r.h.s of Eq. 5 (corresponding to uniform distribution) is dropped, we obtain the differential correlation function $Diff(r)$, containing only the structural contribution to the distribution function. Summarizing, the comparison between experimental and model data will be carried out using both $QI(Q)M(Q)$ and $Diff(r)$, while for the discussion of the model characteristics we will use both $g_{ij}(r)$ and $Diff(r)$, depending on the distance range considered. All the above functions were calculated form the MD trajectories using in-house codes purposely written.

IR measurements

The Fourier transform infrared (FTIR) measurements were performed with a Bruker 66V FTIR spectrometer. We measured the transmittance spectra from the Far-IR (FIR) to the Mid-IR (MIR) (30-5000 cm^{-1}). For the FIR region we used a Mylar beamsplitter and a room temperature DLATGS (deuterated L-alanine doped triglycene sulphate) detector. THe MIR region was investigated through a Potassium Bromide (KBr) beam splitter and a Mercury Cadmium Tellurium (MCT) detector working at 77K.

A Bruker cell equipped with zinc telluride (ZnTe) and polyethylene windows having a variable path length from 0.020 to 0.010 mm was used for the IR measurements in transmission. The cell was positioned in the sample compartment of the interferometer in the focus of an f/4 parabolic mirror and the transmitted beam was collected by a twin mirror and then focused onto the detector. The empty cell was used as reference in the measurements and the transmittance $T(\nu)$ (where ω is the frequency in cm^{-1}) has been calculated as $T(\omega)=I(\omega)/I_0(\omega)$, where $I_0(\omega)$ ($I(\omega)$) is the intensity transmitted by the empty (filled with the ionic liquid) cell. Finally, for each spectrum 128 scans were recorded at a spectral resolution of 4 cm^{-1}.

Computational Details

In order to provide a full characterization of the structure of the liquid within the relevant range of radial distances that are accessible to experiments, we have performed three different simulations of the bulk system composed by an equal number of [Ala] anions and [Cho] cations. The first simulation is an *ab initio* MD performed by means of the CP2k program on a bulk system composed by 55 ionic pairs of IL. A pre-equilibration was performed employing classical molecular dynamics within periodic boundary conditions, using the AMBER program package[26] and the Gaff force field.[27,28] The partial atomic charges have however been recomputed owing to the RESP method using the B3LYP electronic

density. The resulting charges have been scaled by 0.8 to roughly account for polarization effects. Pre-equilibration took 1 ns of physical time and the simulation temperature was set at 350 K. The starting configurations that resulted from this procedure were used to set up ab initio molecular dynamics simulations with the program package CP2K,[29] using the Quickstep module[30] and the orbital transformation[31] for faster convergence. The electronic structure was calculated by means of the PBE[32] functional, with an explicit Van der Waals correction that includes the empirical dispersion correction (D3) by Grimme.[33] Basis sets of the kind MOLOPT-DZVP-SR-GTH and GTH pseudopotentials[34,35] were used. The time step was chosen to be 0.5 fs and the simulation temperature was set to 350 K using the Nosé-Hoover chain thermostat. The cell side-length was set to 25.57 Å for a density of 1.05 g/cm^3 (experimental 1.08 g/cm^3). After 5 ps of equilibration, a 32 ps production trajectory in the NVT *ensemble* was performed. During the simulation, every 5 timesteps, the Wannier centers[36] of the whole system have been computed in order to obtain the IR spectra.

A second trajectory has been produced by means of the CPMD program[37] using the CPMD dynamics and a smaller configuration that included only 12 ionic couples and a cell with 15.32 Å box length for a density of 1.06 g/cm^3 (experimental 1.08 g/cm^3). Also in this simulation we have used the PBE functional (this time without dispersion corrections), Troullier-Martin pseudopotentials,[38] a cutoff of 80 Ry and a timestep length of 4 a.u. (about 0.097 fs). The cell has been equilibrated for 14 ps using a Berendsen thermostat[39] while the production stage lasted 27 ps and was subjected to a Nosé-Hoover thermostat[40] at room temperature in the NVT *ensemble*.

A third MD simulation has been performed by means of the previously mentioned Gaff force field on a large cubic cell with a side length of 43 Å containing 300 ionic couples. The classical MD production trajectory has been generated for 2 ns in the NVT ensemble at constant density of 1.14 g/cm^3 that is the density to which the Gaff force field equilibrates.

Results and discussion

Structure

The first relevant result that can be extracted form our trajectories is the static structure factor. This quantity, which provides us a general idea of the liquid structure, can be used as a probe of the accuracy of the calculations when directly compared to the experimental measurement. We present a comparison of the X-ray static structure factor $QM(Q)I(Q)$ calculated from the two *ab initio* simulations and the corresponding experimental measurement in the upper panel of Figure 2. A complementary quantity that can help in the understanding of the liquid structure is the $Diff(r)$ function as calculated through Eq. 5. This quantity is presented in the lower panel of Figure 2.

As expected, we have a nearly perfect agreement between the simulated and theoretical patterns on all range both for $QI(Q)M(Q)$ and $Diff(r)$. Few minor differences can be easily spotted for the peaks at 2 and between 3 and 4 Å^{-1}. As we shall see below, this is a critical region where we find the typical distances due to the interaction between the oxygen atoms of the ionic couple partners, O[Ala]-O[Cho], and those due to the interaction of the carboxylate with the nitrogen atom of choline, O[Ala]-N[Cho]. The former interaction between the oxygen atoms is mediated by an HB, while the second interaction is mediated by strong electrostatic forces between the negatively charged atoms of the carboxylate and the positively charged, nitrogen atom of the ammonium group of choline. The differences between the two *ab-initio* sets of data in the same region are probably due to the different treatment of the dispersion corrections that have been include only in the simulation performed with CP2k.

We highlight a few important features that stem from the static structure factor:

- the presence of a principal peak falling around 1.5 Å^{-1};
- presence of two smaller peaks (resembling shoulders) at 2.3 and 3.6 Å^{-1};
- the absence of the pre-peak at lower Q that clearly points to a lack of long range

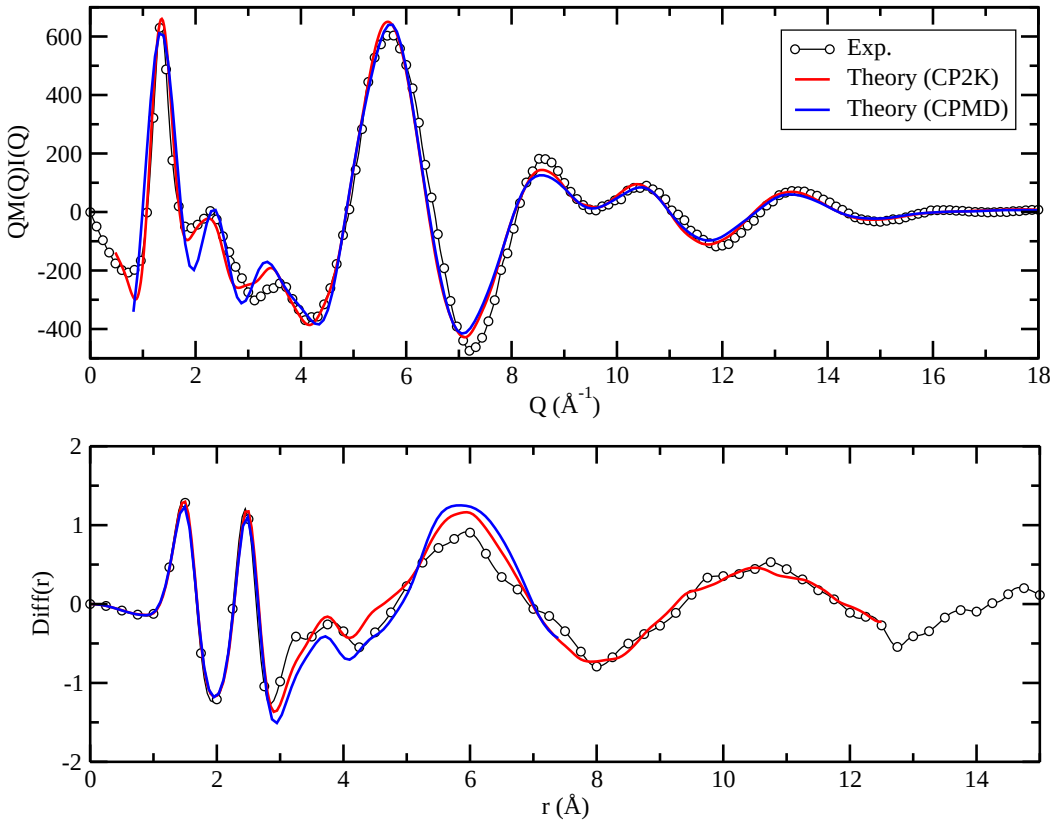

Figure 2: Upper panel: Choline Alanine $QI(Q)M(Q)$ experiments (circles) and theory (CPMD in red and CP2k in blue). Lower panel: the Fourier transform of the $QI(Q)M(Q)$ data gives rise to the $Diff(r)$ function.

structures in the liquid

The strong feature at 1.5 $Å^{-1}$ is compatible with the typical structure of ionic liquids that presents an alternating, albeit irregular pattern of cations and anions. This peak is compatible with the average distance between the cation and the anion center of mass (c.o.m.) which falls in a broad range between 4 and 7 Å . More precisely this peak arises from the spatial correlation between carbon atoms on different ions. The two shoulders at 2.3 and 3.4 $Å^{-1}$ correlate with distances of 2.7 and 1.8 Å . The first is in the range of anion-cation intermolecular interactions mediated by an hydrogen bond, while the second is probably due to intramolecular spatial correlations.

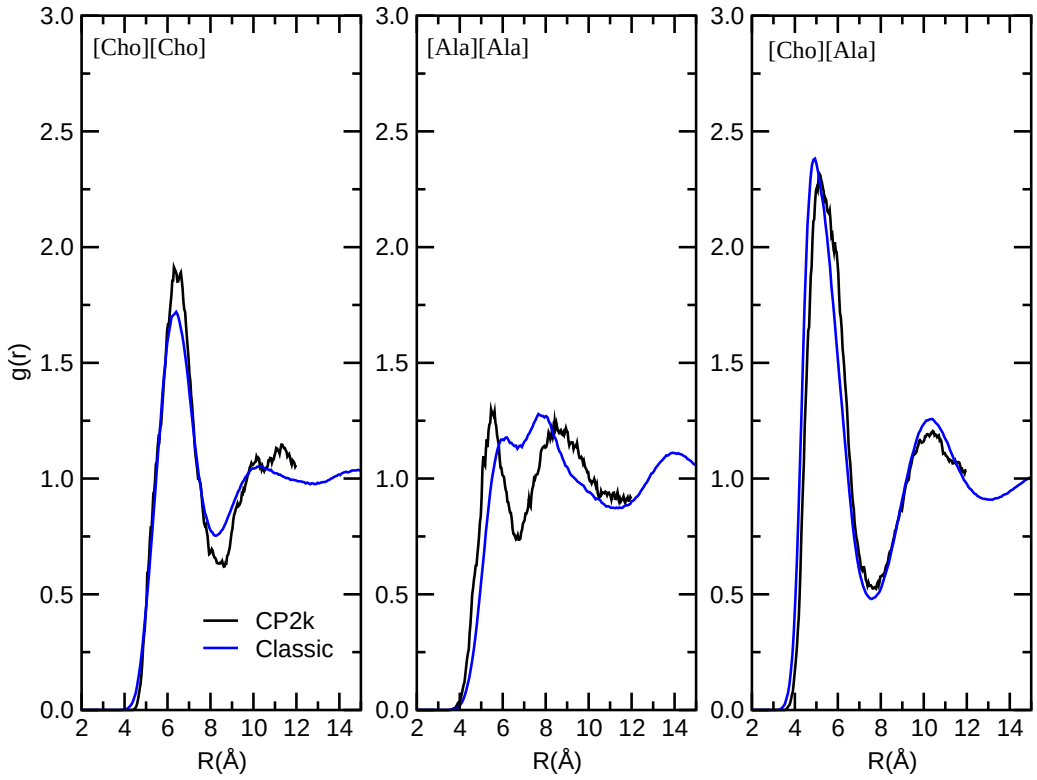

Figure 3: Cation-anion (right), cation-cation (middle) and anion-anion (left) radial distribution functions for their center of masses (RDFs). Results from classical (blue line) and *ab-initio* (black line) MD

The $g(r)$ between the center of mass of cations and anions is reported in Figure 3. As

we can see in the right panel of Figure 3, the first shell of cations surrounding the anions (and viceversa) has a density maximum at around 5 Å , while the peak of the spatial correlations between anions (middle panel) and between cations (left panel) move to slightly larger distances and therefore give rise to feature located at smaller Q. The strong peak at 6 Å in the $Diff(r)$ function (in the lower panel of Figure 2) might be attributed to cation-anion correlations and to anion-anion correlation whose RDF's present maxima in the region between 5 and 6 Å . In the same plot we see a broad feature at long range at about 10 Å which might be due to anion-cation correlation in the second shell as pointed out by a second peak between 10 ans 12 Å in their relevant RDF as reported by the left panel of Figure 3.

As we pointed out above, the experimental data show clearly the absence of any peak below the main one in the structure factor. This feature points to the absence of any long range structure that is, instead, a very common feature of other ILs. Unfortunately, the side lengths of our *ab-initio* simulation cells are too small to provide reliable data in the pre-peak region below 1 $Å^{-1}$. For this reason we have also extracted the structure factor from the classical simulation where the cell side length allows us to obtain data down to 0.3 $Å^{-1}$. In Figure 4 we report a comparison of the experimental data with the the $QI(Q)M(Q)$ obtained using the classical MD simulation employing the Gaff force field. As it can be easily seen from Figure 4, most of the important features are actually very well described at the classical level even if we are using a general force field with static charges. The MD simulations reported here shows clearly (in agreement with the experimental data) the absence of any structure beyond 12-15 Å as shown by the absence of any feature in the low-Q region below 1 $Å^{-1}$. This is extremely important as many other ionic liquids have been shown to present long-range structures even in the absence of long alkyl chains (see ref.[7] for an example).

The inter-molecular radial distribution functions (RDFs) between the most representative atoms of cation(choline) and anion(alanine) are given in Figure 5 where we show the results

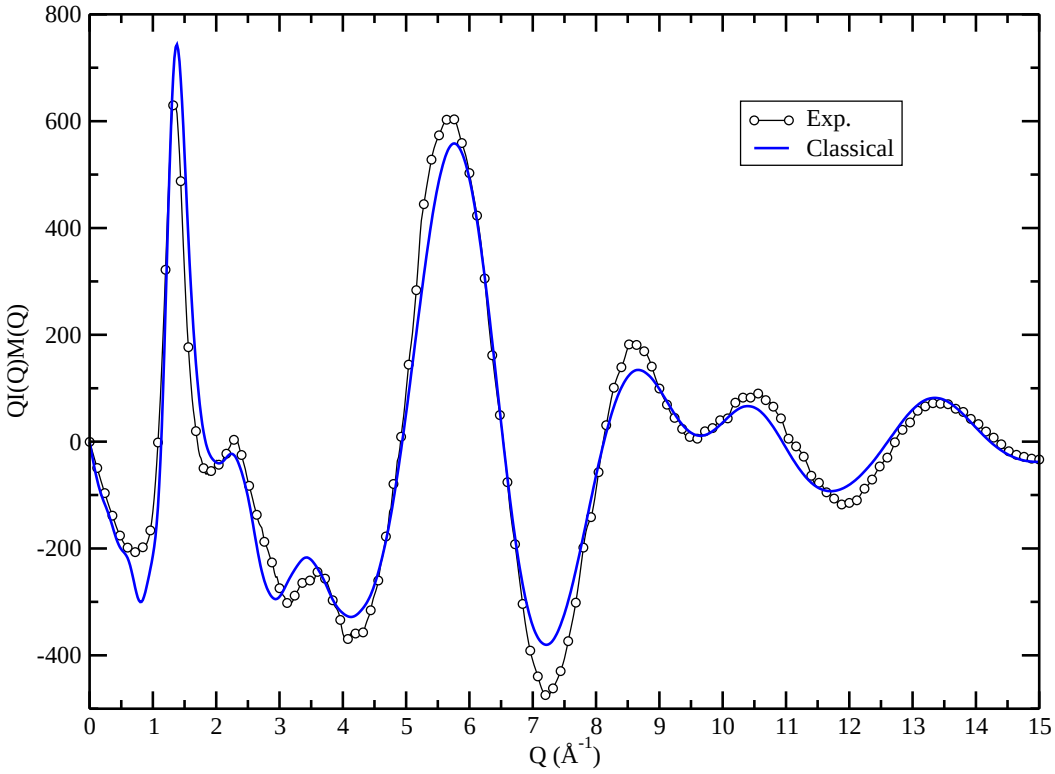

Figure 4: Upper panel: Choline Alanine $QI(Q)M(Q)$ experiments (empty circles) and classical MD dynamics (blue line).

obtained with both *ab initio* MD and the Classical MD results.

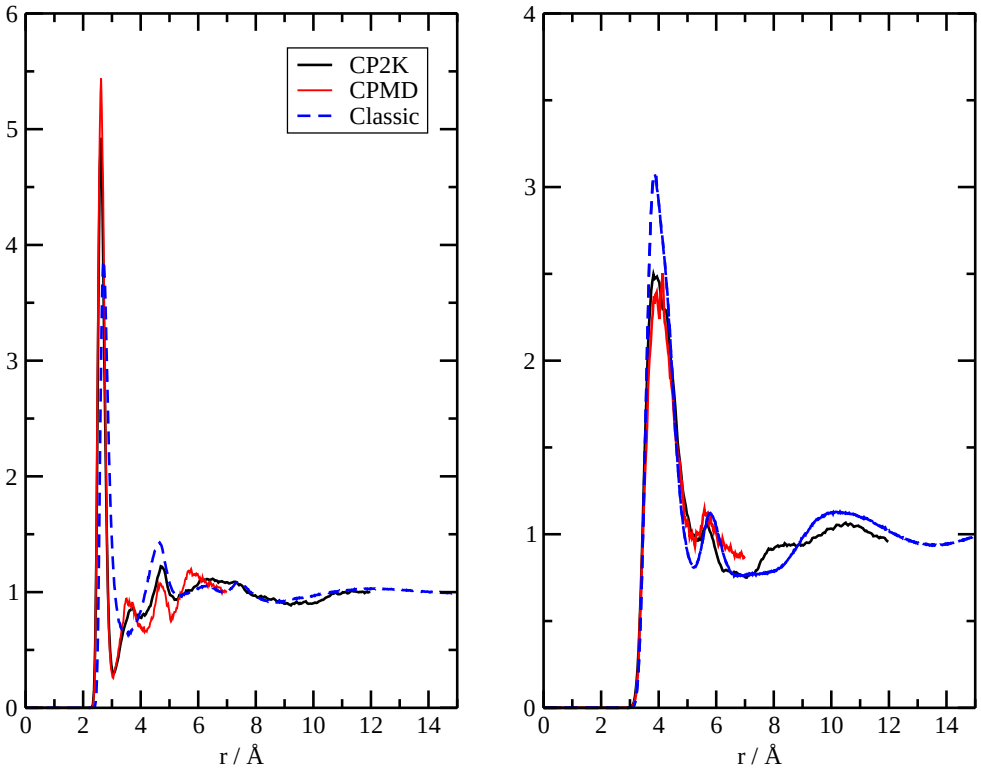

Figure 5: Atomic radial distribution functions (RDFs): (A) oxygen atoms of anions and oxygen atoms of the cation. (B) nitrogen atoms of cations and oxygen atoms of anions.Three sets of data are reported including the data from the two ab initio MD and then ones from classical dynamics.

The left panel of Figure 5 presents the RDF between the oxygen atoms of anion and the oxygen atoms of the cation. From the well defined maximum of the curve, which is found at around 2.60 Å , it can be inferred that the carboxylate group of anion forms a strong hydrogen bond with the hydroxyl group of cation. This equilibrium distance value is in good agreement with that obtained from the single IL couple by Benedetto et al.[41] The structure beyond the main peak that consists of two small peaks around 4-5 Å is due to the the "bidentate" nature of the carboxylate group that is the HB acceptor. The symmetry of the carboxylate terminals leads to a complex patterns of possible positions of the donor oxygen

atoms of the choline cation (see below). By looking at the data in Figure 5, we see that the performance of the classical Gaff force field in this particular system is extremely accurate and capable of grasping most of the structural features and substantially reproducing the *ab initio* patterns.

The right panel of Figure 5 presents the RDFs between nitrogen atoms of cations and oxygen atoms of anions. This RDF shows a broad peak centered at about 4 Å. This correlation is due to the electrostatic interaction between the negative charges on the oxygen atoms and the positive charge localized on the ammonium nitrogen and has already been noticed in the gas phase equilibrium structures.[41] The presence of a well structured peak in the RDF between the nitrogen atoms on $[Cho]^+$ and the oxygen on $[ALA]^-$ is an important structural feature that shows, once again, how the present IL is substantially structured by means of an alternating pattern of anions and cations that retains many of the characteristics of the isolated ion pairs.

In Figure 6, we show in more detail the double coordination between the cation and anion that is due to both the HB and the above electrostatic interaction of the carboxylate with the [Cho] N atom. In particular, we show a combined RDF that relates two different distances: r_1. the distance O[Cho]$\cdots$O[Ala] and r_2, the distance O[Ala]$\cdots$N[Cho] as indicated in the the sketch on the left of Figure 6. The bidimensional plot clearly shows the presence of one distinctive peak located at 2.5 Å on r_1 that correlates with the r_2 distance with a distribution that has a maximum between 4 and 6 Å . The correlation between the two distances is seen to exists only for the first peak of the O[Cho]$\cdots$O[Ala] distribution therefore showing that the carboxylate group of alanine behaves as a bi-dentate terminal that has a double interaction with choline at the same time: one through the HB with oxygen and the other with the N atom. The O(alanine)$\cdots$N(alanine) interaction is however weaker then the one coming from the O(alanine)$\cdots$O(alanine) contact.

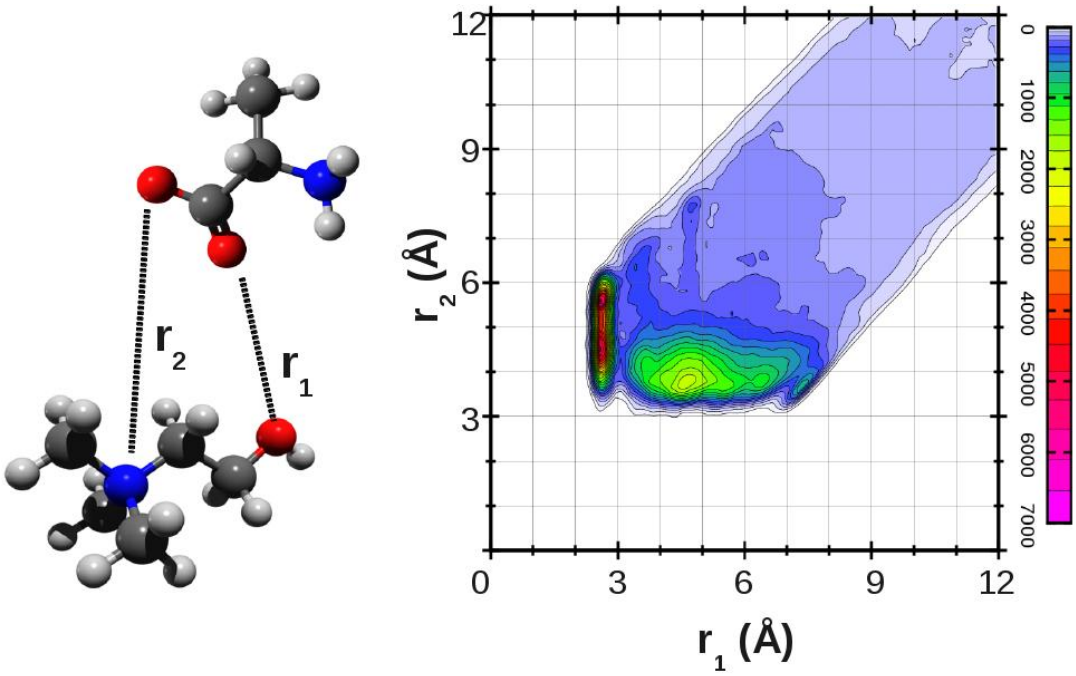

Figure 6: Left Panel: CDF showing the double interaction between cation and anion. Left Panel: the two coordinates considered for the Combined Distribution Function (CDF) analysis. Right: CDF as a contour plot. Colors indicate different occcurence values (legend far right)

HB features

In order to provide an better visual picture of the structure of the atoms involved in the hydrogen bonding we have calculated the Spatial Distribution Functions (SDF) of hydrogen and oxygen atoms around the anion and the cation. The results are reported in Fig. 7. The data presented here have been extracted from the CPMD simulation, but those obtainable from the CP2K trajectory are essentially very similar.

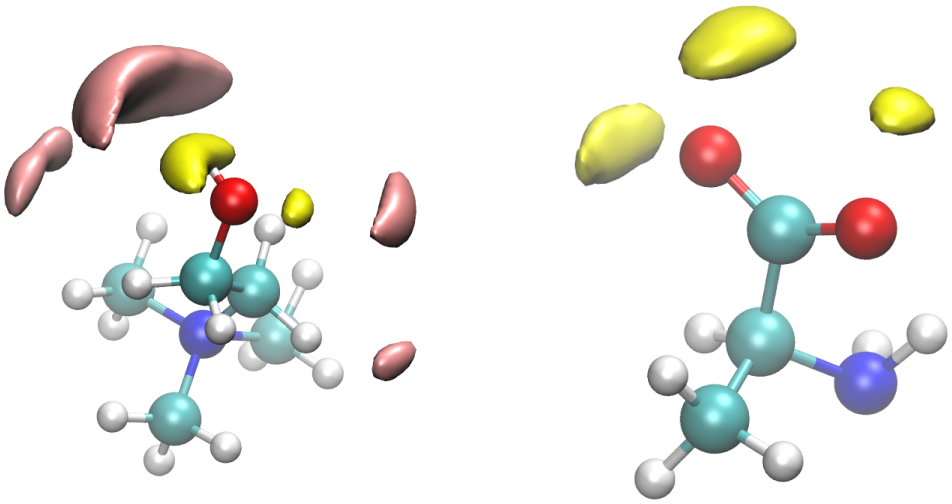

Figure 7: Left: the choline structure is plotted with the density of its proton (yellow) and that of the alanine oxygen (pink). Right: the alanine strcuture is plotted with the density of the choline proton (yellow). In each plot the surface has been drawn so to include roughly 70% of the density.

The proton is well localized between the carboxylate terminal (which is the acceptor) of the [Ala] anion and the oxygen of the [Cho] cation (which is the donor). Obviously, due to the symmetry of the carboxylate acceptor there are various location once a frame of reference has been selected to match three atoms of [Ala]. It is interesting to note that when

one oxygen of the carboxylate terminal has been involved in the HB, the other can also be coordinated, albeit to a smaller extent, in a second HB.

It is interesting to compare the above findings of the *ab initio* MD with those coming from the classical MD that employs the *Gaff* force field. The SDF of the atoms involved in the HB are reported in Figure 8. As can be easily noticed from the comparison between Figure 8 and the quantum results of Figure 7, the classical trajectory agrees in the overall structure of the H-bonding complex. The classical trajectory presents obviously a more averaged configuration, owing to the longer simulation times.

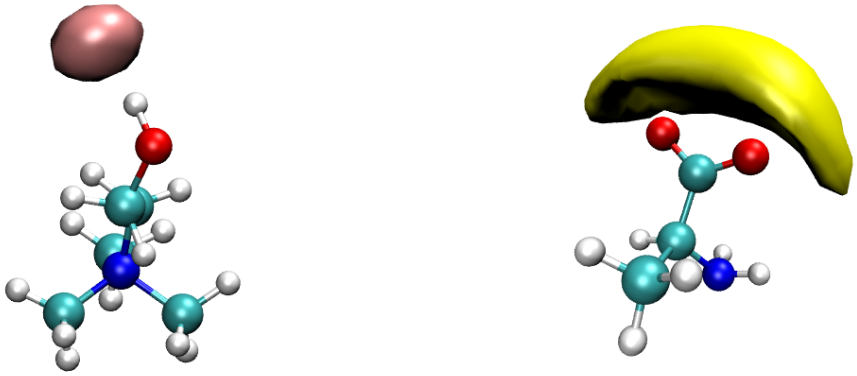

Figure 8: Left: Choline with the alanine oxygen density (pink). Right: alanine with the density of the acidic proton of choline (yellow). In each plot the surface has been drawn so as to include roughly 50% of the density.

In order to inspect the dynamics of HBs we report in Figure 9 a series of O[Ala]-H[Cho] distances as they evolve with time during the CPMD simulation. In each panel the time evolution of the distance is reported for each of the 12 alanine molecules, but we have limited

the plot to the short range distances in order to focus on the H-bonding distance region. As one can see, there are two alanine molecules that do not form any HB with choline during our simulation time. In most of the other panels, instead, we see the alanine molecule forming one unique strong HB (with distances around 1.5 Å). In these cases there is always a double coordination with the other carboxylate oxygen with distances around 3-4 Å. As we can see from panels 6, 7, and 10, the two ends of the carboxylate can exchange their role during the dynamics. During the rather limited time of our simulations we have detected only one double HB that is depicted in panel 11. The magenta and red line represent a coordination with a single carboxylate group of the same alanine molecule. The black line is an HB formed with a second molecule of alanine. This peculiar case sees the presence of a shared HB between two different choline molecules, one of which rotates its hydroxyl group during the dynamics.

In order to check whether the double features of the HBs depicted in Figure 9 are really involving the dynamics of a single HB, we have recalculated the HB dynamics by taking the distance between the geometric center between the two carboxylate oxygen and the oxygen atom of choline. The results are reported in Figure 10 in a fashion similar to what we have seen above. We see that for most of the ionic couples involved there is only one HB with a O-O distance between 3 and 4 Å. Two of the alanine molecules (panels 8 and 9) do not form a strong HB during the simulation and two of them seem to be able form a double HB with two different choline molecules (panels 5 and 11).

In order to further investigate the ability of the classical force field to reproduce the H-bonding feature on these systems we present the HB count (normalized to the number of ionic couples) as a function of the simulation time in Figure 11. Since the CP2K simulation has been performed at 350 K we have excluded it from this comparison. The total simulation time has been set to 1 for ease of comparison. The number of HB has been counted using the following convention: the acceptor-donor distance must be less than 3.0 Å and the $\hat{\text{OHO}}$ must be at least 150°.

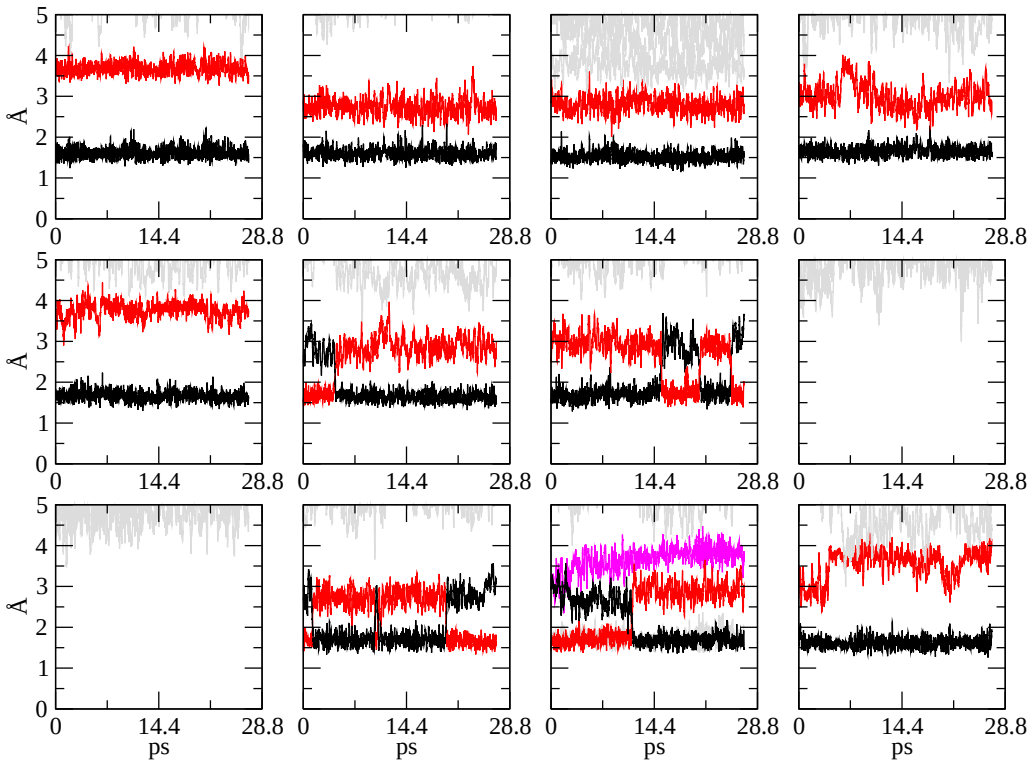

Figure 9: Time development of the O(ala)-H(choline) distance. See main text for details.

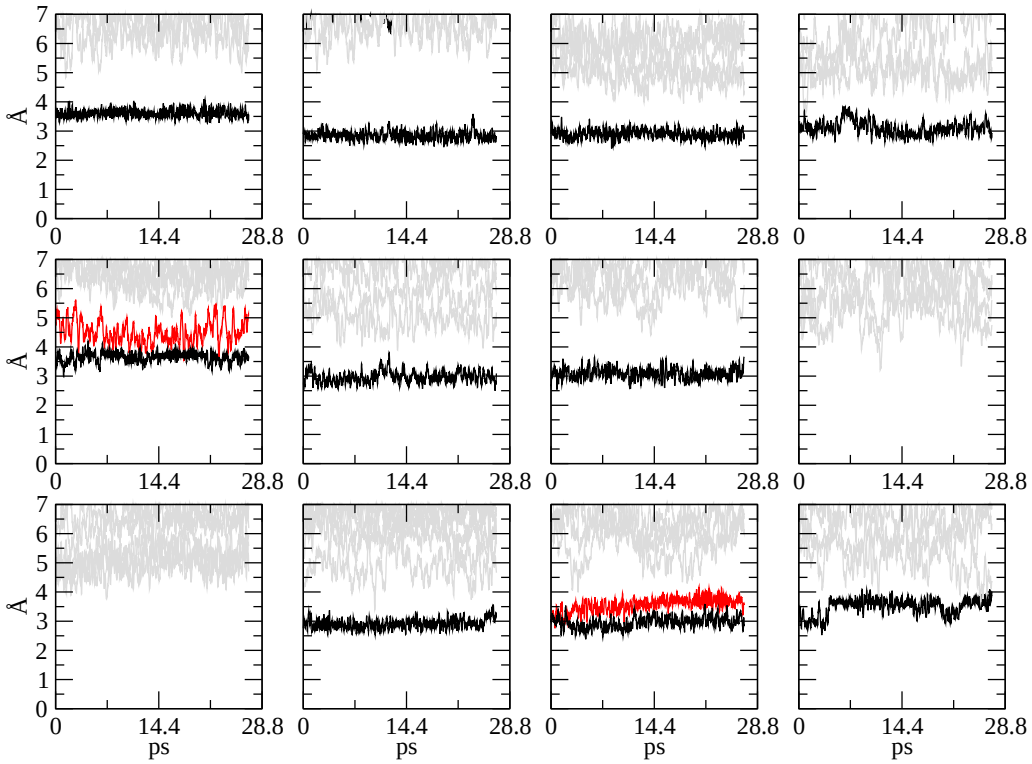

Figure 10: Time development of the distance between the geometric center of carboxylate and the choline oxygen atom. See main text for details.

As we can see, the number of HBs predicted to exist in the classical simulation is substantially less than those that we find in the *ab initio* CPMD trajectory. In particular we find that the average number of HBs per ion pair in the CPMD trajectory is 0.7 while it turns out to be 0.6 in the classical trajectory. It is likely that the *Gaff* force fields, not including polarization, underestimates the strength of the HBs interactions. Anyway the prediction that we obtain from the classical trajectory is remarkably close to the *ab-initio* results therefore showing that in first approximation the system under study can be well described by a static charge non polarizable force field.

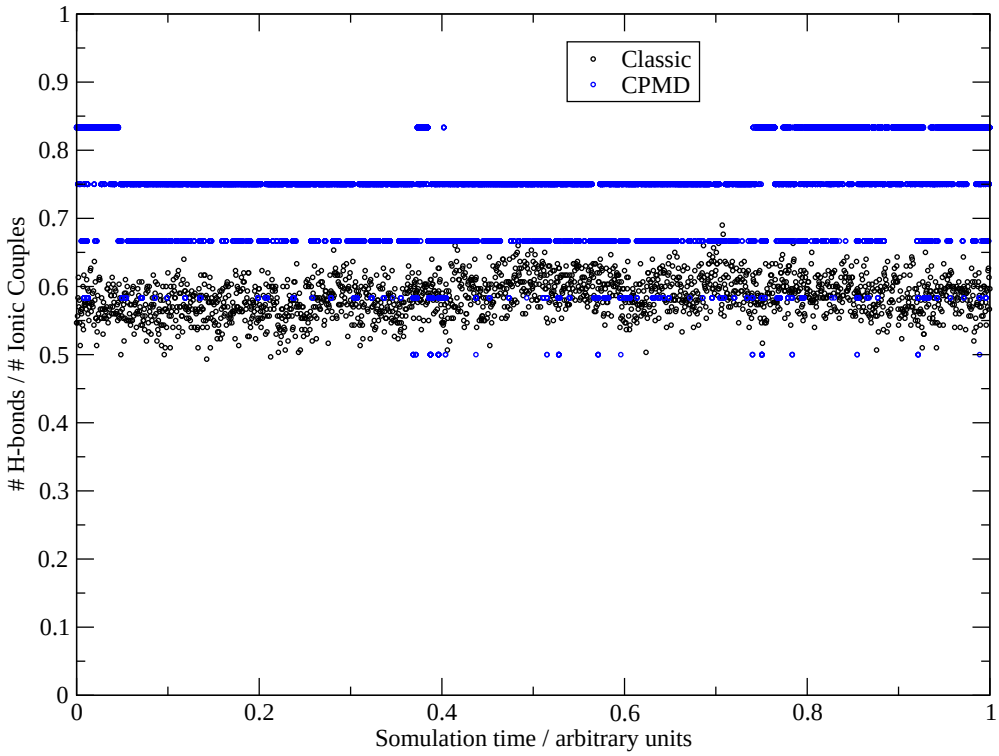

Figure 11: Number of O-H-O hydrogen bonds per ionic couple as a function of simulation time (renormalized to one).

IR spectra

The last analysis we present here is the calculation of the IR spectra. Since we are dealing with a bulk liquid, we cannot apply the usual direct calculation based on the Hessian diagonalization to obtain the relative vibrational frequencies and therefore we employed the methods implemented in the TRAVIS package[42] based on the Fourier transform of the autocorrelation of molecular dipole moments which has the advantage, owing to the *ab-initio* nature of the involved forces, to account for anharmonicity.

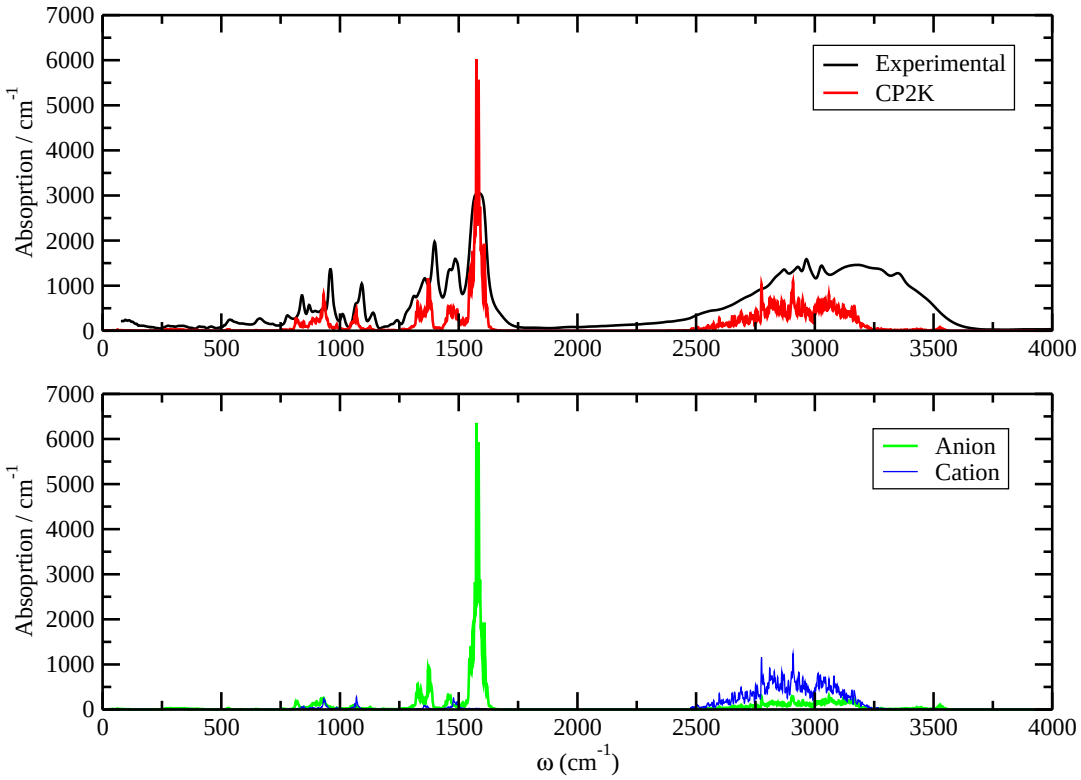

Figure 12: Upper Panel: experimental (black line) vs. theoretical (red line) IR spectra. Lower Panel: Partial contribution to total IR spectra of cation (blue line) and anion (green line) molecules.

In Figure 12 we report the comparison between IR theoretical spectra as calculated from the CP2K simulation and the experimental one. In the lower panel we have shown separately the two contributions coming from the cation and anion molecules. In general we have found

a very good agreement between our predicted data and the experimental spectra over all the frequency range. From the lower panel of Figure 12, we can infer that the major contribution to the total IR spectra, especially for low ω values, derives from anions. As expected, in fact, such molecules are more IR active due to the presence of the polar carboxylate group.

As a further insight in the interpretation of the IR spectra we show in Figure 13 a comparison between the computed spectra from the CP2K simulation, the one that arise from the harmonic approximation in the isolated ion pairs that we have already presented in our previous paper on these systems[41] and the experimental data. The assignment of some of the most prominent peaks on the experimental pattern has been performed using as a reference both the normal modes from the harmonic approximation and by using the MOLSIM package[43] where the FT of the velocity autocorrelation of all atoms was calculated and projected onto a likely choice of normal modes. The results of this analysis are schematically reported in Table 1 we show a comparison of the positions of the main experimental peaks against the theoretical data and their assignment. We have limited the results to the "fingerprint" region from 700 cm^{-1} to 1700 $cm^{-}1$. Obviously the prominent features are due to the absorptions of the carboxyl group (asymmetric and symmetric stretching motions) that fall around 1380 and 1580 cm^{-1}.

Regarding the higher frequency range ($\omega > 2000$ cm^{-1}), we can see a very broad band in both experimental and simulated spectra, that is due to the numerous H-X (X=C,N) stretching vibrations superposed onto each other that include the O-H stretching of [Cho]. While the former have rather localized distribution functions, the hydroxyl vibration presents a broad range of absorption frequencies (2500-3400 cm^{-1}), owing to the wide distribution of hydrogen bond energies and conformations that is very typical of protic liquids.

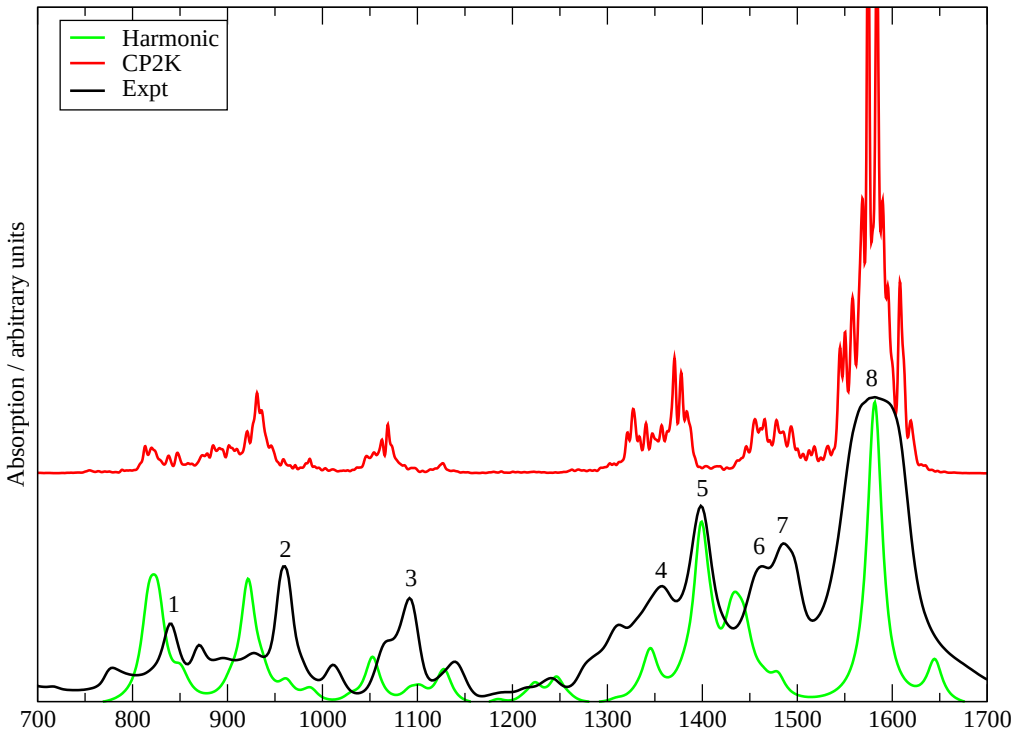

Figure 13: Comparison of the theoretical IR spectra as obtained from the CP2K simulation on the bulk liquid (red line), theoretical spectra in the harmonic approximation from the study of the isolated partner species from the data in[41] (scaled by the usual 0.95 factor, green line) and experimental data (black line).

Table 1: Assignment of vibrational modes of and of experimental peak values, for $700 < \omega < cm^{-1}$. Frequencies are in cm^{-1}.

Mode	Expt. freq.	CP2K	Harmonic	Assign.
1	840	814	820	HB bend.
2	961	931	922	NH_2 wag.
3	1091	1072	1053	CH_n rock./twist.
4	1358	1336	1344	C-H bend. [Ala]
5	1399	1379	1398	CO_2^- symm str.
6	1461	1457	1434	various CH_n sciss.
7	1487	1477	1476	CH_3 sciss. [Cho]
8	1581	1575	1582	CO_2^- asymm str.

Conclusions

In this work we have presented a joined experimental-computational study of a biocompatible room temperature ionic liquid, namely choline-alaninate, at ambient conditions. The X-Ray diffraction patterns and the infrared spectra, collected here for the first time, have been successfully interpreted with both classical and *ab initio* molecular dynamics simulations, the latter also used to model the measured infrared absorption spectra of the liquid through VDOS-Wannier centers calculations. The dynamics of the bulk liquid has been explored, within the obvious spatial and temporal limits of the exploited models, by means of three different computational choices: (i) a pure-DFT plane wave calculation using Car -Parrinello dynamics, (ii) a pure DFT, mixed basis, calculation within the Born-Oppenheimer scheme with CP2k and (iii) a classical molecular dynamics using the *Gaff* force field. The various molecular dynamics simulations presented here converge clearly to the same liquid structure and the computational results are in excellent agreement with the corresponding experimental quantities. Our study highlights the existence of very strong hydrogen bonds between cations and anions and no evidence of a medium-range spatial order and of the corresponding pre-peaks in the structure factor. The typical oxygen-oxygen interaction mediated by the HB strongly binds the ionic couple partners in the liquids phase providing structures that are reminiscent of those that we have found in a gas-phase, *ab-initio* geometrical optimization of the isolated ionic couple. The acceptor-donor distance turns out to be 2.6 Å with the proton localized exclusively on the Choline hydroxyl. Our dynamics simulations show that, within the temporal limits of the simulation, no proton transfer occurs and that once formed the HB strongly binds a single ionic couple in such a way that the coupling is persistent along the simulation and a cation anion exchange takes place only seldom if ever. Moreover, the strong HB interaction gives origin to a very broad O-H stretching absorption profile that is localized between 2500 and 3500 cm^{-1} in agreement with the experimental data. A noteworthy result is that the most important structural features of the liquid can be modeled using the simple two body *Gaff* force field with very small adjustment encouraging a further development of

the same force field to provide a general framework for the structural description of all the series of analogue liquids based on different aminoacids.

Acknowledgement

The authors are deeply grateful to Pietro Ballone, for his support and for the very helpful discussions. Financial support of the Scientific Committee of the University of Rome through grants C26A13KR5Z, C26A142SCB and C26H13MNEB is gratefully acknowledged. Computational support from Cineca (grant n. IsC11_ESP-IL) and PRACE (grant n.2013091962) is also acknowledged.

References

(1) Wilkes, J. S. A short history of ionic liquids-from molten salts to neoteric solvents. *Green Chem.* **2002**, *4*, 73–80.

(2) Castner, E. W.; Wishart, J. F. Spotlight on ionic liquids. *J. Chem. Phys.* **2010**, *132*, 120901.

(3) Wasserscheid, P.; Keim, W. Ionic liquids - new "solutions" for transition metal catalysis. *Angew. Chem., Int. Ed.* **2000**, *39*, 3772–3789.

(4) Zaitsau, D. H.; Kabo, G. J.; Strechan, A. A.; Paulechka, Y. U.; Tschersich, A.; Verevkin, S. P.; Heintz, A. Experimental Vapor Pressures of 1-Alkyl-3-methylimidazolium Bis(trifluoromethylsulfonyl)imides and a Correlation Scheme for Estimation of Vaporization Enthalpies of Ionic Liquids. *J. Phys. Chem. A* **2006**, *110*, 7303–7306.

(5) Dong, K.; Zhang, S. Hydrogen Bonds: A Structural Insight into Ionic Liquids. *Chemistry Eur. J.* **2012**, *18*, 2748–2761.

(6) Bodo, E.; Sferrazza, A.; Caminiti, R.; Mangialardo, S.; Postorino, P. A prototypical ionic liquid explored by ab initio molecular dynamics and Raman spectroscopy. *J. Chem. Phys.* **2013**, *139*, 144309.

(7) Gontrani, L.; Bodo, E.; Triolo, A.; Leonelli, F.; D'angelo, P.; Migliorati, V.; Caminiti, R. The Interpretation of Diffraction Patterns of Two Prototypical Protic Ionic Liquids: a Challenging Task for Classical Molecular Dynamics Simulations. *J. Chem. Phys. B* **2012**, *116*, 13024–13032.

(8) Caminiti, R., Gontrani, L., Eds. *The structure of Ionic Liquids*; Softand Biological Matter; Springer, 2014; Vol. 193.

(9) Gao, Y.; Arritt, S. W.; Twamley, B.; Shreeve, J. M. Guanidinium-Based Ionic Liquids. *Inorg. Chem.* **2005**, *44*, 1704–1712.

(10) Nockemann, P.; Thijs, B.; Driesen, K.; Janssen, C. R.; Van Hecke, K.; Van Meervelt, L.; Kossmann, S.; Kirchner, B.; Binnemans, K. Choline Saccharinate and Choline Acesulfamate: Ionic Liquids with Low Toxicities. *J. Phys Chem. B* **2007**, *111*, 5254–5263.

(11) Fukaya, Y.; Iizuka, Y.; Sekikawa, K.; Ohno, H. Bio ionic liquids: room temperature ionic liquids composed wholly of biomaterials. *Green Chem.* **2007**, *9*, 1155–1157.

(12) Yu, Y.; Lu, X.; Zhou, Q.; Dong, K.; Yao, H.; Zhang, S. Biodegradable Naphthenic Acid Ionic Liquids: Synthesis, Characterization, and Quantitative Structure–Biodegradation Relationship. *Chemistry Eur. J.* **2008**, *14*, 11174–11182.

(13) Plaquevent, J.-C.; Levillain, J.; Guillen, F.; Malhiac, C.; Gaumont, A.-C. Ionic Liquids: New Targets and Media for α-Amino Acid and Peptide Chemistry. *Chem. Rev.* **2008**, *108*, 5035–5060.

(14) Petkovic, M.; Ferguson, J. L.; Gunaratne, H. Q. N.; Ferreira, R.; Leitao, M. C.; Sed-

don, K. R.; Rebelo, L. P. N.; Pereira, C. S. Novel biocompatible cholinium-based ionic liquids-toxicity and biodegradability. *Green Chem.* **2010**, *12*, 643–649.

(15) Costa, A. J. L.; Soromenho, M. R. C.; Shimizu, K.; Marrucho, I. M.; Esperança, J. M. S. S.; Lopes, J. N. C.; Rebelo, L. P. N. Density, Thermal Expansion and Viscosity of Cholinium-Derived Ionic Liquids. *ChemPhysChem* **2012**, *13*, 1902–1909.

(16) Weaver, K. D.; Kim, H. J.; Sun, J.; MacFarlane, D. R.; Elliott, G. D. Cyto-toxicity and biocompatibility of a family of choline phosphate ionic liquids designed for pharmaceutical applications. *Green Chem.* **2010**, *12*, 507–513.

(17) Moriel, P.; García-Suárez, E.; Martínez, M.; García, A.; Montes-Morán, M.; Calvino-Casilda, V.; Bañares, M. Synthesis, characterization, and catalytic activity of ionic liquids based on biosources. *Tetrahedron Letters* **2010**, *51*, 4877 – 4881.

(18) Fukumoto, K.; Yoshizawa, M.; Ohno, H. Room Temperature Ionic Liquids from 20 Natural Amino Acids. *J. Am. Chem. Soc.* **2005**, *127*, 2398–2399.

(19) Tao, G.-h.; He, L.; Liu, W.-s.; Xu, L.; Xiong, W.; Wang, T.; Kou, Y. Preparation, characterization and application of amino acid-based green ionic liquids. *Green Chem.* **2006**, *8*, 639–646.

(20) Liu, Q.-P.; Hou, X.-D.; Li, N.; Zong, M.-H. Ionic liquids from renewable biomaterials: synthesis, characterization and application in the pretreatment of biomass. *Green Chem.* **2012**, *14*, 304–307.

(21) Hou, X.-D.; Liu, Q.-P.; Smith, T. J.; Li, N.; Zong, M.-H. Evaluation of Toxicity and Biodegradability of Cholinium Amino Acids Ionic Liquids. *PLoS ONE* **2013**, *8*, e59145.

(22) Albertini, V. R.; Bencivenni, L.; Caminiti, R.; Cilloco, F.; Sadun, C. A new technique for the study of phase transitions by means of energy dispersive x-ray diffraction. Application to polymeric samples. *J. Macromol. Sc. B* **1996**, *35*, 199–213.

(23) Carbone, M.; Caminiti, R.; Sadun, C. Structural study by energy dispersive X-ray diffraction of amorphous mixed hydroxycarbonates containing Co, Cu, Zn, Al. *J. Mater. Chem.* **1996**, *6*, 1709–1716.

(24) Atzei, D.; Ferri, T.; Sadun, C.; Sangiorgio, P.; Caminiti, R. Structural Characterization of Complexes between Iminodiacetate Blocked on Styrene-Divinylbenzene Matrix (Chelex 100 Resin) and Fe(III), Cr(III), and Zn(II) in Solid Phase by Energy-Dispersive X-ray Diffraction. *J. Am. Chem. Soc.* **2001**, *123*, 2552–2558.

(25) Gontrani, L.; Russina, O.; Marincola, F. C.; Caminiti, R. An Energy Dispersive X-Ray scattering and Molecular Dynamics study of liquid dimethyl carbonate. *J. Chem. Phys.* **2009**, *131*, 244503.

(26) Case, D. A. et al. AMBER 12. 2012; `http://ambermd.org/`.

(27) Wang, J.; Wolf, R. M.; Caldwell, J. W.; Kollman, P. A.; Case, D. A. Development and testing of a general amber force field. *J. Comp. Chem.* **2004**, *25*, 1157–1174.

(28) Wang, J.; Wang, W.; Kollman, P. A.; Case, D. A. Automatic atom type and bond type perception in molecular mechanical calculations. *J. Mol. Graph. Mod.* **2006**, *25*, 247 – 260.

(29) Hutter, J.; Iannuzzi, M.; Schiffmann, F.; VandeVondele, J. cp2k: atomistic simulations of condensed matter systems. *WIREs Comput Mol Sci* **2013**, n/a.

(30) Vandevondele, J.; Krack, M.; Mohamed, F.; Parrinello, M.; Chassaing, T.; Hutter, J. QUICKSTEP: Fast and accurate density functional calculations using a mixed Gaussian and plane waves approach. *Comp. Phys. Comm.* **2005**, *167*, 103–128.

(31) VandeVondele, J.; Hutter, J. An efficient orbital transformation method for electronic structure calculations. *J. Chem. Phys.* **2003**, *118*, 4365–4369.

(32) Madsen, G. K. H. Functional form of the generalized gradient approximation for exchange: The PBE alpha functional. *Phys. Rev. B* **2007**, *75*, 195108+.

(33) Grimme, S. Semiempirical GGA-type density functional constructed with a long-range dispersion correction. *J. Comp. Chem.* **2006**, *27*, 1787–1799.

(34) Goedecker, S.; Teter, M.; Hutter, J. Separable dual-space Gaussian pseudopotentials. *Phys. Rev. B* **1996**, *54*, 1703–1710.

(35) Hartwigsen, C.; Goedecker, S.; Hutter, J. Relativistic separable dual-space Gaussian pseudopotentials from H to Rn. *Phys. Rev. B* **1998**, *58*, 3641–3662.

(36) Marzari, N.; Vanderbilt, D. Maximally localized generalized Wannier functions for composite energy bands. *Phys. Rev. B* **1997**, *56*, 12847–12865.

(37) Andreoni, W.; Curioni, A. New Advances in Chemistry and Material Science with CPMD and Parallel Computing. *Parallel Computing* **2000**, *26*, 819–842.

(38) Troullier, N.; Martins, J. L. Efficient pseudopotentials for plane-wave calculations. *Phys. Rev. B* **1991**, *43*, 1993–2006.

(39) Berendsen, H. J. C.; Postma, J. P. M.; van Gunsteren, W. F.; Dinola, A.; Haak, J. R. Molecular dynamics with coupling to an external bath. *J. Chem. Phys.* **1984**, *81*, 3684–3690.

(40) Hoover, W. G. Canonical dynamics: Equilibrium phase-space distributions. *Phys. Rev. A* **1985**, *31*, 1695–1697.

(41) Benedetto, A.; Bodo, E.; Gontrani, L.; Ballone, P.; Caminiti, R. Amino Acid Anions in Organic Ionic Compounds. An ab Initio Study of Selected Ion Pairs. *J. Phys Chem. B* **2014**, *118*, 2471–2486.

(42) Brehm, M.; Kirchner, B. TRAVIS - A Free Analyzer and Visualizer for Monte Carlo and Molecular Dynamics Trajectories. *J. Chem. Inf. and Mod.* **2011**, *51*, 2007–2023.

(43) Buchbauer, G.; Klinsky, A.; Weiß-Greiler, P.; Wolschann, P. Ab initio Molecular Electrostatic Potential Grid Maps for Quantitative Similarity Calculations of Organic Compounds. *J. Mol. Mod.* **2000**, *6*, 425–432.